Thomson scattering diagnostic for study fast events in the TEXTOR plasma

M.Yu. Kantor[1,2,3], G. Bertschinger[3], P. Bohm[4], A. Buerger[1,3], A.J.H. Donné[1], R. Jaspers[1], A. Krämer-Flecken[3], S. Mann[1], S. Soldatov[3], Zang Qing[5] and the TEXTOR Team[3]

[1]*FOM-Institute for Plasma Physics Rijnhuizen*, Association EURATOM-FOM, P.O. Box 1207, 3430 BE Nieuwegein, The Netherlands*
[2]*Ioffe Institute, RAS, Saint Petersburg 194021, Russia*
[3]*Institute for Energy Research – Plasma Physics*, Forschungszentrum Jülich GmbH, Association EURATOM-FZJ, D-52425 Jülich, Germany*
[4] *Institute of Plasma Physics AS CR, 182 00 Prague 8, Czech Republic*
[5]*Institute of Plasma Physics, Chinese Academy of Sciences, Hefei 230031, China*
**Partners in the Trilateral Euregio Cluster*

1. Introduction

Thomson scattering (TS) is a reliable diagnostic which provides local electron temperature and density profiles of the plasma. One of the important challenges of a TS diagnostic is to enhance the measurement repetition frequency to study fast events in plasma, like sawteeth, plasma disruptions, ELMs etc. Basically two different routes are explored: using several lasers firing within a short time interval [1,2] or, as will be described here, using multi-pass intra-cavity systems [3, 4, 5, 6] providing from a single laser a burst of several tens of laser pulses generated at a repetition frequency up to 20 kHz.

Recently, a multi-pass intra-cavity laser probing system has been implemented on the TEXTOR tokamak [6]. This report presents the design of the system, the test of its efficiency and a few examples of fast events measured in the TEXTOR plasma by the upgraded diagnostic.

2. Design of multi-pass intra-cavity laser probing system on TEXTOR.

The TS diagnostics on the TEXTOR tokamak (R=1.75 m, a=0.47 m) was designed to study fast plasma dynamics in the sub-millisecond time scale at a spatial resolution less than a centimeter. First, the diagnostic operated with a double-pass intra-cavity laser probing system; in 2008 it was upgraded with a 6-pass system [6] and several months later the number of passes was increased up to 12.

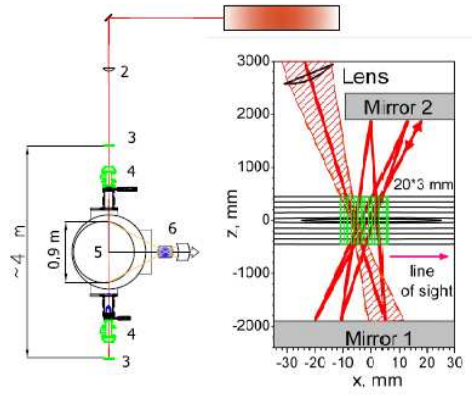

Fig. 1.
Layout of the 12-pass laser probing system at TEXTOR
1. Laser table, 2. Focusing lens, 3. Spherical mirrors, 4. Brewster laser ports, 5. Plasma, 6. Collection lens and fiber bundle input.

The layout of the laser probing system on TEXTOR is shown in Fig. 1. A laser oscillator consisting of a single ruby rod (19 mm diameter) is installed on an optical table (1) at a distance of ~10 m from the tokamak. The laser beam generated in the oscillator is focused in the plasma centre by lens (2), and passes the plasma volume (5) several times reflecting from two spherical mirrors (4) of 1900 mm curvature radii and returns back in to the laser oscillator. The system was tuned so that the multi-pass system and the rear mirror on the laser table form a stable laser cavity [7]. In this case, the long laser cavity has a minimum of diffraction losses of laser light and all laser beams are focused in the plasma centre having waists of similar dimensions.

The scattered light is collected by objective (6) from a 90 cm long chord, covering the full plasma diameter, and transferred via a fiber bundle to a Littrow grating spectrometer. Spectrally resolved images are detected by a fast Phantom V7.0

CMOS camera [5]. The camera collects a number of 12 bit images of 512*384 pixels size at 10 kHz frame rate. Images with Thomson scattered light alternate with net plasma light, so one camera enables TS measurements at a 5 kHz repetition rate.

The insertion in Fig. 1 shows the path of the laser beam in the 12-pass probing system. The input beam is shown together with its envelope and waist. The horizontal scale is significantly enlarged with respect to the vertical one to make the beam path better visible. The plasma volume scanned by the zigzagging laser beam is shown by the green hatched rectangles. In the figure plane it is 900*20 mm in size and <3 mm deep. The circular magnetic surfaces of the plasma are plotted by black solid lines and appear nearly horizontally in the selected scale. Scattered light is collected nearly tangential to the plasma magnetic surfaces. This provides a spatial resolution of the diagnostics across the magnetic surfaces of better than 1 cm [6].

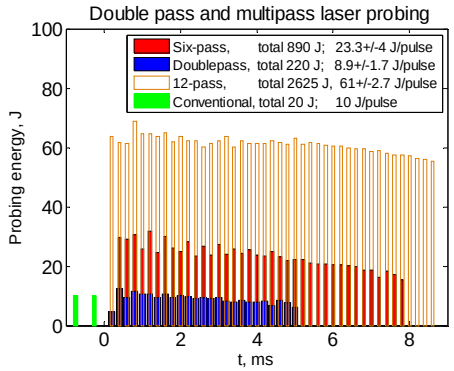

Fig. 2
Laser pulse probing energies

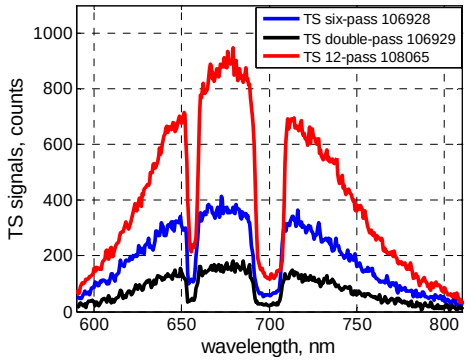

Fig. 3
TS scattered signals

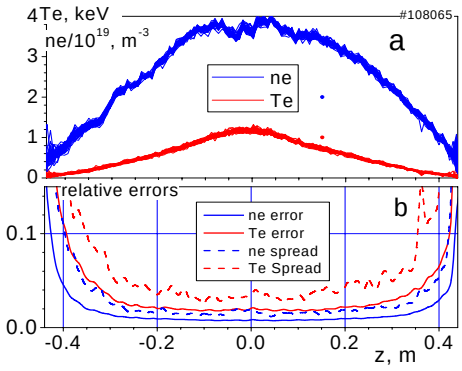

Fig. 4
TS measurements with 12-pass system
a. T_e and n_e profiles
b. relative errors and data spreads

3. Efficiency of the multi-pass laser probing system on TEXTOR.

The effect of the multi-pass system on the laser output pulse train is shown in Fig. 2. The double-pass system is compared with the six- and twelve-pass systems. The multi-pass system provides a proportional increase of the pulse probing energy in the plasma as compared to the double-pass system. The decrease of the returned beam energy with the number of passes shows the light losses per single pass to be ~2.5%, which is attributed to reflection and scattering losses from the Brewster windows.

The multi-pass probing made it possible to extend the duration of the pulse train up to 9 ms keeping a high pulse energy level. The total integrated probing energy of all useful laser pulses was increased from ~200 to more than 2500 Joules.

Note, that a conventional ruby laser system is capable to provide only a couple of laser pulses with ~10 J of probing energy each [8], which are shown here also for comparison.

The effect of the multi-pass probing on the scattered signals is shown in Fig. 3. These scattered spectra from double-, six-pass and twelve-pass laser probing were measured in similar plasma discharges at a central plasma density of ~$3*10^{19}$ m^{-3}. The two dips in the spectra correspond to the masked H line at 656 nm and to the blocked ruby laser line at 694 nm.

The 12-pass probing improves the statistical error of the TS measurements in a single laser pulse in respect to the double-pass probing by a factor of 3: from 6% to 2% for temperature and from 3% to 1% for density measurement in the plasma core. Fig. 4a presents electron temperature and density profiles measured with the 12-pass systems during 9 ms at steady state plasma

conditions and plotted in two sets of the red and blue curves. Actually, there are 43 overlapped profiles in the sets measured in individual laser pulses. The profiles are hardly distinguished because of a specially selected quiet phase of plasma discharge and a high accuracy of TS measurements.

The relative temperature and density measurement errors are shown by the red and blue solid curves in Fig. 4b. A higher accuracy of density measurements has been achieved by normalizing the line averaged density measured by the TS diagnostic along the probing axis to that measured by the HCN interferometer along the same chord shifted by 45° in the toroidal direction at 10 kHz sampling rate and at ~0.1% accuracy [9]. A time delay between the TS and HCN measurements were taken into account when it was necessary.

For the double- and six-pass systems the statistical errors correspond well to the standard deviations of electron temperature and density measured in a laser burst. With the 12-pass system, the statistical errors appeared less then the data deviations (dash curves in Fig. 4b) even in quiet steady state plasma. This can be an indication of small fluctuations in the plasma parameters related particularly to plasma turbulence [10].

4. Measurements of fast plasma events with the multi-pass TS system.

The new capabilities of the multi-pass TS diagnostic are illustrated here by measurements of the evolution of the electron temperature and density during fast events in TEXTOR plasma.

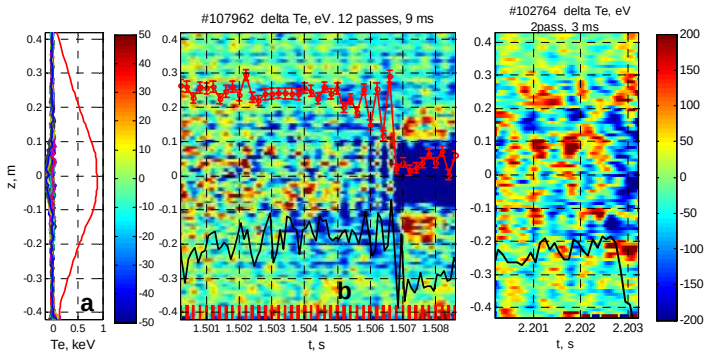

Fig. 6
Evolution of T_e before and after sawtooth crash
a. Averaged T_e profile and its time variations,
b. 2D plot of Te variations,
c. Te variations measured with the double pass system.

Fig. 5 shows the evolution of the electron temperature measured by the TS diagnostic along the full plasma chord before and after a sawtooth crash. The averaged temperature profile before the crash is shown in Fig 6a along with the temperature variations in individual laser pulses with 12-pass laser probing. The time-space domain of these variations in Fig. 5b reveals the structure of the oscillations with a resolution as high as 10 eV. One can see the precursor of the crash as a periodical oscillation of the central temperature which corresponds to that measured by electron cyclotron emission (ECE) shown by the black curve. The oscillation of the averaged temperature measured by TS is shown by the red curve with error bars. The precursor is followed by the crash. The temperature in the central plasma region is quenched and the heat is expelled to the periphery. A similar event measured with the double-pass system (fig. 5c) demonstrates the advantage of the multi-pass probing.

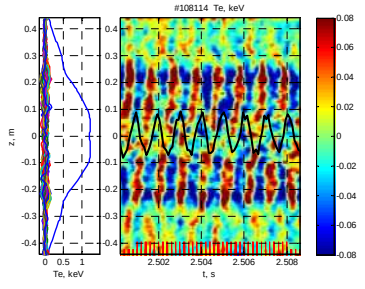

Fig. 6a
T_e oscillation in islands

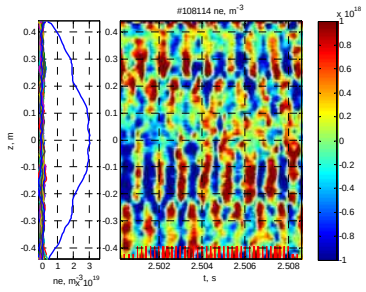

Fig. 6b
n_e oscillation in islands

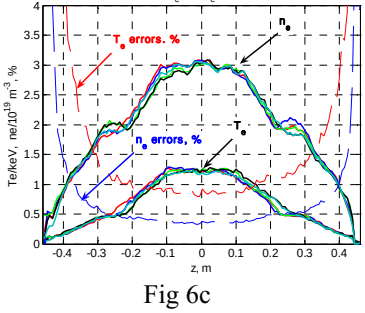

Fig 6c
T_e and n_e profiles in 0.2 ms step

Another illustration of the performance of the TS diagnostic is the measurements of rotating islands induced by a helical AC current in the Dynamic Ergodic Diverter (DED) in TEXTOR [11]. The space-time domains of small electron temperature and density variations along with their profiles taken in 0.2 ms time steps are shown in Fig. 6.

The temperature variations have a pronounced helical structure which is attributed to the plasma rotation The largest oscillations (±15%) are located at z=±23 cm inside the q=2 magnetic surface. At the q=2 surface (z=±28 cm) the temperature variations become minimal indicating the position of m/n=2/1 magnetic island in plasma. The temperature oscillations are synchronized with the ECE signal measured the near island region and shown in Fig. 6a by the black curve.

In the island region the relative density oscillations achieve a maximum level of ±5% (Fig. 6b). The density is peaked inside the islands which are clearly seen in Fig.6c presenting the dynamics of the T_e and n_e profiles measured in 123 spatial points and plotted in 0.2 ms time intervals. The measurement accuracy of the profiles is shown in the plot as well.

The final example is a study of electron heat transport during ECRH. Fig. 7 shows the dynamics of the electron pressure just after switch on of 600 kW of ECRH power with the EC resonance located inside the q=1 surface at z=±7 cm. Electron heating starts immediately after ECRH power switch on (red vertical line in Fig. 7a) and the absorbed energy is perfectly confined inside the q=1 surface during the first 5 ms of the heating. Nevertheless, the electron heating rate inside the q=1 surface calculated from the local TS data shows ~200 kW (Fig. 7b) which is only one third of the launched EC power. This discrepancy could be an indication of fast degradation of the electron energy confinement at the start of ECRH or violation of a maxwellian electron velocity distribution. These two possible explanations are under experimental study in TEXTOR with the upgraded TS diagnostic.

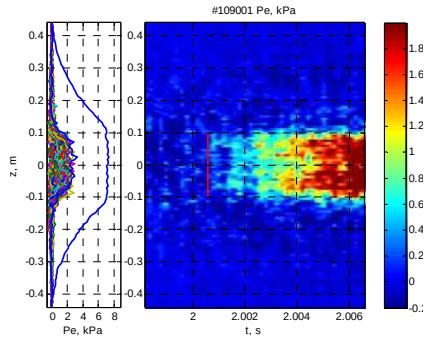

Fig. 7a
Evolution of electron pressure variation at the start of ECRH

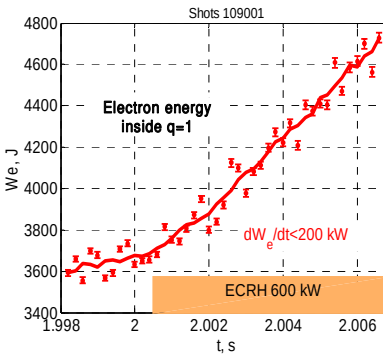

Fig. 7b
Electron heating inside q=1 surface during ECRH

Acknowledgments

This work was supported by NWO-RFBR Centre-of-Excellence grant 047.018.002. This work, supported by the European Communities under the Contract of Association between EURATOM-FOM, was carried out within the framework of the European Fusion Programme. The views and opinions expressed herein do not necessarily reflect those of the European Commission.

1 M.J.Walsh et al. Rev. Sci. Instr. 74 (2003) 16663
2 T.N.Carlstrom et al. Rev. Sci. Instrum. 63 (1992) 4901
3 M.Y.Kantor and D.V.Kouprienko. Techn. Phys. Lett. 23 (1997) 321
4 M.Yu.Kantor and D.V Kouprienko. Rev. Sci. Instrum. 70 (1999) 780
5 H.J. van der Meiden et al. Rev. Sci. Instrum. 75 (2004) 3849
6 M.Yu.Kantor et al. Plasma Phys. Control. Fusion, 51 (2009) 055002
7 M.Yu.Kantor. Techn. Phys. Lett. 25 (1999) 860
8 M.N.A. Beurskens et al. Rev. Sci. Instrum. 68 (1997) 721
9 A. J. H. Donné et al, Fusion Sci. Techn. 47 (2005) 220
10 L.Vermare et al. Nucl. Fusion, 46 (2006) S743
11 Special Issue, Fusion Eng. Design 37 (1997) 335, edited by K.H. Finken.